

JGR Planets

RESEARCH ARTICLE

10.1029/2020JE006602

Key Points:

- Measured 15, 20, 40, 50, and 100 eV emission cross sections of Cameron Bands (CO) and 1NG Bands (CO⁺) from electron impact fluorescence of CO
- Developed rovibrational spectral models of Cameron Band, 1NG, and 4PG systems based upon optically thin middle ultraviolet laboratory spectra of e + CO
- Measured lifetime of the CO(a³Π) state to be 3 ± 1 ms

Correspondence to:

J. M. Ajello,
joe.ajello@lasp.colorado.edu











Citation:

Lee, R. A., Ajello, J. M., Malone, C. P., Evans, J. S., Veibell, V., Holsclaw, G. M., et al. (2021). Laboratory study of the Cameron bands, the first negative bands, and fourth positive bands in the middle ultraviolet 180–280 nm by electron impact upon CO. *Journal of Geophysical Research: Planets*, 126, e2020JE006602. <https://doi.org/10.1029/2020JE006602>

Received 1 JUL 2020

Accepted 16 NOV 2020

Laboratory Study of the Cameron Bands, the First Negative Bands, and Fourth Positive Bands in the Middle Ultraviolet 180–280 nm by Electron Impact Upon CO

Rena A. Lee^{1,2} , Joseph M. Ajello¹ , Charles P. Malone³ , J. Scott Evans⁴ ,
Victoir Veibell⁴ , Gregory M. Holsclaw¹ , William E. McClintock¹ , Alan C. Hoskins¹,
Sonal Jain¹ , Jean-Claude Gérard⁵ , and Nicholas M. Schneider¹ 

¹Laboratory for Atmospheric and Space Physics, University of Colorado, Boulder, CO, USA, ²Now at Earth and Planetary Sciences, School of Ocean and Earth Sciences and Technology, University of Hawaii, Honolulu, HI, USA, ³Jet Propulsion Laboratory, California Institute of Technology, Pasadena, CA, USA, ⁴Computational Physics Inc., Springfield, VA, USA, ⁵University of Liège, Liège, Belgium

Abstract We have analyzed medium-resolution (full width at half maximum, FWHM = 1.2 nm), Middle UltraViolet (MUV; 180–280 nm) laboratory emission spectra of carbon monoxide (CO) excited by electron impact at 15, 20, 40, 50, and 100 eV under single-scattering conditions at 300 K. The MUV emission spectra at 100 eV contain the Cameron Bands (CB) CO(a³Π → X¹Σ⁺), the fourth positive group (4PG) CO(A¹Π → X¹Σ⁺), and the first negative group (1NG) CO⁺(B²Σ⁺ → X²Σ) from direct excitation and cascading-induced emission of an optically thin CO gas. We have determined vibrational intensities and emission cross sections for these systems, important for modeling UV observations of the atmospheres of Mars and Venus. We have also measured the CB “glow” profile about the electron beam of the long-lived CO (a³Π) state and determined its average metastable lifetime of 3 ± 1 ms. Optically allowed cascading from a host of triplet states has been found to be the dominant excitation process contributing to the CB emission cross section at 15 eV, most strongly by the d³Δ and a³Σ⁺ electronic states. We normalized the CB emission cross section at 15 eV electron impact energy by multilinear regression (MLR) analysis to the blended 15 eV MUV spectrum over the spectral range of 180–280 nm, based on the 4PG emission cross section at 15 eV that we have previously measured (Ajello et al., 2019, <https://doi.org/10.1029/2018ja026308>). We find the CB total emission cross section at 15 eV to be 7.7 × 10^{−17} cm².

Plain Language Summary Carbon monoxide (CO) is an important molecule in the atmospheres of many planetary bodies, including Mars and Venus. These two planets have nearly identical UV spectra, exhibiting CO, CO₂, and N₂ as dominant components of the upper atmospheres. Thorough investigation of atmospheric emissions relies on spectral models of individual emission features, which depend on laboratory-based measurements of the emission cross sections and metastable lifetimes. In this paper, we trace the history of the emission cross section work for electron impact on CO, identify previous experimental systematic flaws, and present corrected values for the emission cross sections of key Middle UltraViolet (MUV; 180–280 nm) emission features over several electron impact energies (15–100 eV). We give special emphasis to the Cameron bands (CBs), the strongest molecular band system in the MUV dayglow observed on Mars. A successful spectral study has neither been accomplished nor been possible until now, with our unique experimental regime at the University of Colorado, which can routinely study optically forbidden transitions. Our emission cross section results for the optically forbidden CB system are vital for increased precision, especially in investigations utilizing electron transport codes (e.g., AURIC, Trans-Mars) to retrieve composition and emission rate measurements in upper atmospheres.

1. Introduction

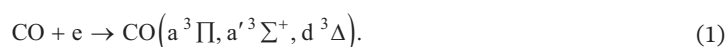
Carbon monoxide is the second most abundant molecule in interstellar space and is used as a tracer for presence of H₂ in star forming regions and molecular clouds (Ferlet et al., 2000; van Dishoeck & Black, 1986). Further, robust laboratory analysis of CO and CO₂ emission features may be an important asset in studying H₂ structures in exoplanetary upper atmospheres, the photolysis of which contributes significantly to at-

atmospheric loss on hydrogen-rich exoplanets (Shematovich et al., 2015). In our solar system, Pluto's atmosphere contains detectable CO and N₂ but lacks CO₂ (Steffl et al., 2020), whereas CO, CO₂, and N₂ are the dominant constituents in the atmospheres of Mars and Venus, which have nearly identical UV spectra (Chaufray et al., 2012; Feldman et al., 2000; Gérard et al., 2017; Hubert et al., 2010). Over the past 50 years, several spacecraft have ventured to Mars to perform remote UV observations from orbit, beginning with Mariner 6, 7, and 9 (Barth et al., 1971, 1972, 1973). More recently, observations of UV emissions have been made by SPICAM on board the Mars Express spacecraft, collecting over 10 million UV spectra (Bertaux et al., 2006). Study of the Martian upper atmosphere expanded further with the Mars Atmosphere and Volatile Evolution (MAVEN) spacecraft Imaging UltraViolet Spectrograph (IUVS) (Jakosky et al., 2015; McClintock et al., 2015) collecting another set of 100,000 spectra since September 2014, gathering airglow data at periaresis consisting of ~12 limb scans for a period of ~22 min for each 4 1/2 h orbit. In early 2021, the Emirates Mars Ultraviolet Spectrometer (EMUS) onboard the Emirates Mars Mission spacecraft will begin orbiting Mars. Upon arrival, EMUS will perform unprecedented Far UltraViolet (FUV; 85–162 nm) imaging of the Mars thermosphere and ionosphere from orbit beginning in late 2021 to expand aeronomical analyses further into the Extreme UltraViolet (EUV; Al Matroushi et al., 2019; Holsclaw, 2020, private communication).

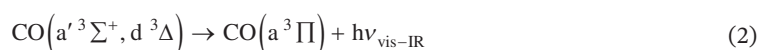
The Middle and Far UltraViolet (MUV and FUV) modeling of the Mars upper atmosphere airglow is presently dependent on electron transport codes such as AURIC (Atmospheric Ultraviolet Radiance Integrated Code) (Evans et al., 2015; Strickland et al., 1999), Trans-Mars (Simon et al., 2009), Monte Carlo (Shematovich et al., 2008), and Boltzmann 3 Constituent (Strickland et al., 1976), which are used to understand the energy input from solar radiation fields (solar wind and solar EUV). Accurate electron impact emission cross sections are the main missing ingredient from ionospheric and cometary forward modeling codes. Many cross sections are unknown or uncertain by a factor of 2 or more (Avakyan et al., 1998; Gérard et al., 2019; Itikawa, 2002; Leblanc et al., 2006, 2007; Simon et al., 2009). This lack of necessary atomic and molecular data jeopardizes accurate altitude determination of minor species (e.g., CO⁺, C, and C⁺) composition and structure interacting with solar radiation field energy inputs (Hubert et al., 2010; Jain et al., 2015). As a first step, electron transport models require spectral models of the individual MUV emissions of the two strongest band systems on Mars: the CO Cameron bands (CB; a ³Π → X ¹Σ⁺) with strongest bands from ~180 to 280 nm and the CO Fourth Positive Group band system (4PG; A ¹Π → X ¹Σ⁺) from 111 to 280 nm. Both band systems can be excited from two abundant gases present on Mars: CO and CO₂. The separation of their gaseous mixing ratios on Mars and Venus, not yet reliably accomplished, awaits a more accurate understanding of the laboratory spectra and electron impact spectra of these two band system emissions and their cross sections from each of these two parent gases.

One of the most experimentally challenging emission spectral features observed on Mars is the optically forbidden CB system resulting from direct excitation and cascade-induced emission of CO and dissociative excitation of CO₂, whose spectrum lies in the MUV. A successful spectral study has neither been accomplished nor been possible until our present laboratory program, which can routinely study optically forbidden transitions such as the CB, the Lyman-Birge-Hopfield (LBH) bands from N₂, or the O i 135.6 nm atomic multiplet from dissociative excitation of CO and CO₂. We have recently made the first step in the far-ultraviolet (FUV; 110–170 nm) studying the 4PG and O i 135.6 nm emission cross sections from both CO and CO₂ (Ajello et al., 2019). The MUV spectral region in the Mars dayglow has not been studied to this level of accuracy in the laboratory because of insufficient experimental vacuum chambers to account for the full MUV CB spectral emission including weak features from 180 to 300 nm and to measure the emission cross section as a function of electron energy.

The electron impact process on CO leading to CB emission is



The excited CO molecules formed in those triplet states at excitation energies both at and above the metastable a ³Π state at 300 K will cascade down into the a ³Π state through dipole-allowed radiative decay maintaining the room temperature rovibrational distribution (Judge & Lee, 1973), that is,



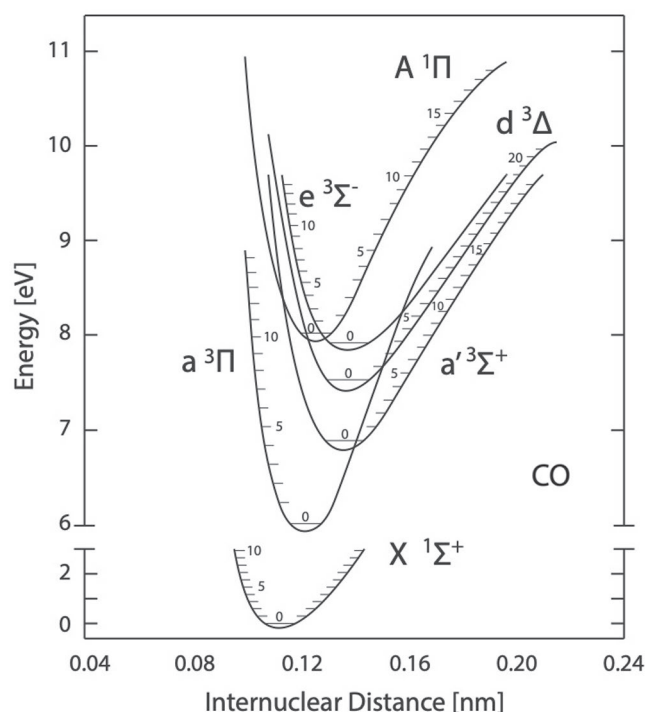
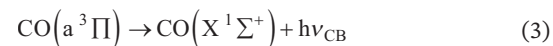


Figure 1. The energy level diagram of CO. Adapted from Herzberg (1970).

followed by



To begin the cross section study, we mention that the CB emission is complicated by significant cascade emissions from these two higher-lying states (see energy level diagram, Figure 1) that provide approximately half the UV emission cross section (Slanger et al., 2008; Zetner et al., 1998).

The process for dissociative excitation of CO₂ leading to CB emission will be discussed in a paper in preparation, since the energetics of the two types of CB direct excitation are very different. The CB system from direct excitation of CO is a CO(*a*³Π → *X*¹Σ⁺) transition with a threshold at 6.01 eV. The CB are a spin-forbidden transition and are excited from CO by an electron exchange process in direct excitation and dipole-allowed cascading. In contrast, the process leading to formation of the *a*³Π from CO₂ is dissociative excitation with a minimum threshold of 11.5 eV with two fragment products: CO(*a*³Π) + O(³P) with the CO(*a*³Π) exhibiting a rotational temperature of over 1000 K (Conway, 1981; Stevens et al., 2015).

All previous experiments of electron-excited CO utilized finite-sized apparatuses with single pixel detectors. Most of these metastable molecules drift out of the field of view as a result of thermal motion. It was shown in the past for N₂ that it is possible to determine what fraction of the total emission cross section is actually observed (Ajello et al., 2017, 2020;

Kanik et al., 2003) by using a large apparatus with an imaging detector, and a knowledge of the velocity distribution and the effective lifetime of the metastable state.

We have started a laboratory aeronomy program at the University of Colorado to study electron impact fluorescence of the CB in the MUV from two parent gases, CO and CO₂, to match and model the spectra of past, present, and future spacecraft equipped with MUV capabilities to observe the upper atmosphere of Mars and Venus (100–300 km) where both gases are present and abundant (Fox, 2008; Gérard et al., 2019; Krasnopolsky & Feldman, 2002). A thorough understanding of CO CB emissions by the same laboratory technique as performed for the LBH bands (Ajello et al., 2020) from a large chamber will lend greater precision in the spectral analysis of solar system objects. These laboratory measurements of both cross sections and spectra are an important step in allowing forward modeling to determine the excitation rates and volume emission rates in the thermospheres of Mars and Venus (Evans et al., 2015; Gérard et al., 2011, 2019; Hubert et al., 2010; Jain et al., 2015; Stevens et al., 2015).

2. History of the Laboratory Study of CB Excitation and Emission Cross Sections

From the existing literature and normalization of early experimental measurements reported by Avakyan et al. (1998), the accepted 15 eV direct excitation cross section of the CB from CO is $1.3 \times 10^{-16} \text{ cm}^2$. This value at 15 eV is attributed to the experimental work of Furlong and Newell (1996) normalized to the theory of Morgan and Tennyson (1993) at 8.5 eV. However, to add complexity to the emission cross section work, Zetner et al. (1998) has shown that the dominant emission low energy cross section to the *a*³Π triplet state arises from cascading from valence electronic states *d*³Δ and *a*'³Σ⁺ ← *X*¹Σ⁺ excitation transitions. Furlong and Newell (1996) recognized that cascade processes are important for the total *a*³Π cross section for energies above 10 eV. This pair of collision processes at 15 eV leads to cascading from the host of triplet states lying above the *a*³Π state shown in Figure 1. For high *v*' levels, the *d*³Δ state with a threshold at 7.4 eV and the *a*'³Σ⁺ state with a threshold at 6.8 eV eventually perturb the vibrational levels of the *A*¹Π state lying at 8.0 eV above the *X*¹Σ⁺ state. We have for the first time resolved this confusing set of direct and cascading excitation cross sections measured by Zetner et al. (1998) leading to the emission cross section measured here for the CB

at 15 eV and other energies from 20 to 100 eV. The A ¹Π state is known to couple to five triplet states leading to an extended FUV + MUV glow from electron excitation of CO by spin-orbit coupling (Ajello et al., 2019).

Comparing several papers, Itikawa (2015) pointed out that the excitation cross sections of the a-state alone are in good agreement at low energy from 6 to 30 eV. First an extensive measurement of the Electron Energy Loss Spectra (EELS) of CO was made by Zobel et al. (1996). These authors obtained absolute values of excitation cross sections for the a ³Π state from threshold to 9.5 eV. Zetner et al. (1998) extended the EELS measurement to obtain the cross section at 10, 12.5, and 15 eV. These two results are consistent with each other. To extend the collision energy further, Zetner et al. (1998) integrated the differential cross sections (DCS) reported at 20 and 30 eV. The same set of excitation cross sections for the prominent cascading states, a' ³Σ⁺ and d ³Δ, are not available.

In the present study, we present emission cross sections, referred to as such because of differences between ours and previous EELS experiments. The CB emission from the a ³Π state is produced by both direct excitation and cascading. For the CO $j \rightarrow m$ transition from the upper state j to a lower state m , the emission cross section σ_{jm}^{em} , including cascade $\sigma_{jm}^{em\ cascade}$, and direct emission $\sigma_{jm}^{em\ direct}$, can be written as

$$\sigma_{jm}^{em} = \sigma_{jm}^{em\ direct} + \sigma_{jm}^{em\ cascade} \quad (4)$$

(Ajello et al., 2019). The mean-free-path of a ³Π for emission in laboratory regimes exceeds any previously employed vacuum chamber used for UV studies (Ajello, 1971a, 1971b). This first and only attempt to measure the e + CO and e + CO₂ CB emission cross section 50 years ago were both significantly flawed as discussed in Erdman and Zipf (1983) and Simon et al. (2009) with an uncertainty of a factor of 2. Erdman and Zipf (1983), for example, performed a partial CB MUV relative intensity study of e + CO from 225 to 265 nm, not including the strongest vibrational features from 180 to 225 nm, and attempted to renormalize the works of Ajello (1971a, 1971b) based on the single CB (1,4) band at 238.9 nm that is blended at low spectral resolution with the 4PG (6,16) feature. The present measurement of the MUV spectrum at 15 eV, and multilinear regression (MLR) modeling to extract both the 4PG and CB systems, resolves this issue of blending from the 4PG band system while providing better modeling of the loss of excited molecules due to the longer lifetime of 3 ms (Section 4.4). Before these current measurements, Erdman and Zipf (1983) recommended an emission cross section of $1.4 \times 10^{-17} \text{ cm}^2$ at 11 eV for the e + CO work of Ajello (1971a, 1971b). We recommend abandoning the previous work of Ajello (1971a, 1971b) based on more accurate work in this experiment, which avoids the effects of uncertainty in spectral blending and includes an accurate accounting for the drift out of the FOV of the a ³Π molecules as measured by the CB glow and the strong triplet system cascade at 15 eV from the work of Zetner et al. (1998).

3. Experimental Apparatus and Procedure

We have measured accurate emission cross sections of two of the strongest optically forbidden transitions found in the Mars airglow: the CB in the MUV (reported in this paper) and O i (135.6 nm) in the FUV (Ajello et al., 2019). We published the initial work 10 years ago for O i (135.6 nm) from dissociation of O₂ using the Cassini UltraViolet Imaging Spectrograph (UVIS) (Kanik et al., 2003; Makarov et al., 2003). In the present study, we have used the MAVEN IUVS Optical Engineering Unit (OEU) “breadboard” flight-spares detector to observe and image the dipole allowed and dipole forbidden emissions occurring in the MUV to more accurately study the CB from electron impact excitation of CO (Ajello, 1971a). No experimental adjustments were made for possible polarization effects, since they are negligible in this case. The polarization fraction for heavier diatomics is generally less than 5%, and for forbidden transitions the fraction would be even smaller (Huschilt et al., 1981; Malone et al., 2008). The experimental apparatus comprised of a large (0.3 m in length) electrostatic electron gun system and the IUVS OEU housed in a large (1.5 m diameter and 2.35 m length) vacuum chamber referred to as the multi-optical beam instrument (MOBI). This experimental setup has been described in detail previously (Ajello et al., 2017; Kanik et al., 2003; Noren et al., 2001), and an experimental schematic is given in Ajello et al. (2017, 2020). The experimental procedure is a replication of Ajello et al. (2019) wherein an electron beam with an energy resolution of ~1 eV was passed through static CO gas with a chamber pressure of 1×10^{-5} Torr ($n = 3 \times 10^{11} \text{ cm}^{-3}$) and gas swarm temperature of 300 K. The cylindrical emission glow profile produced about the electron beam was measured up to a radial distance of ~400 mm, moving upward from the electron beam centered initially at 0 mm, using the IUVS

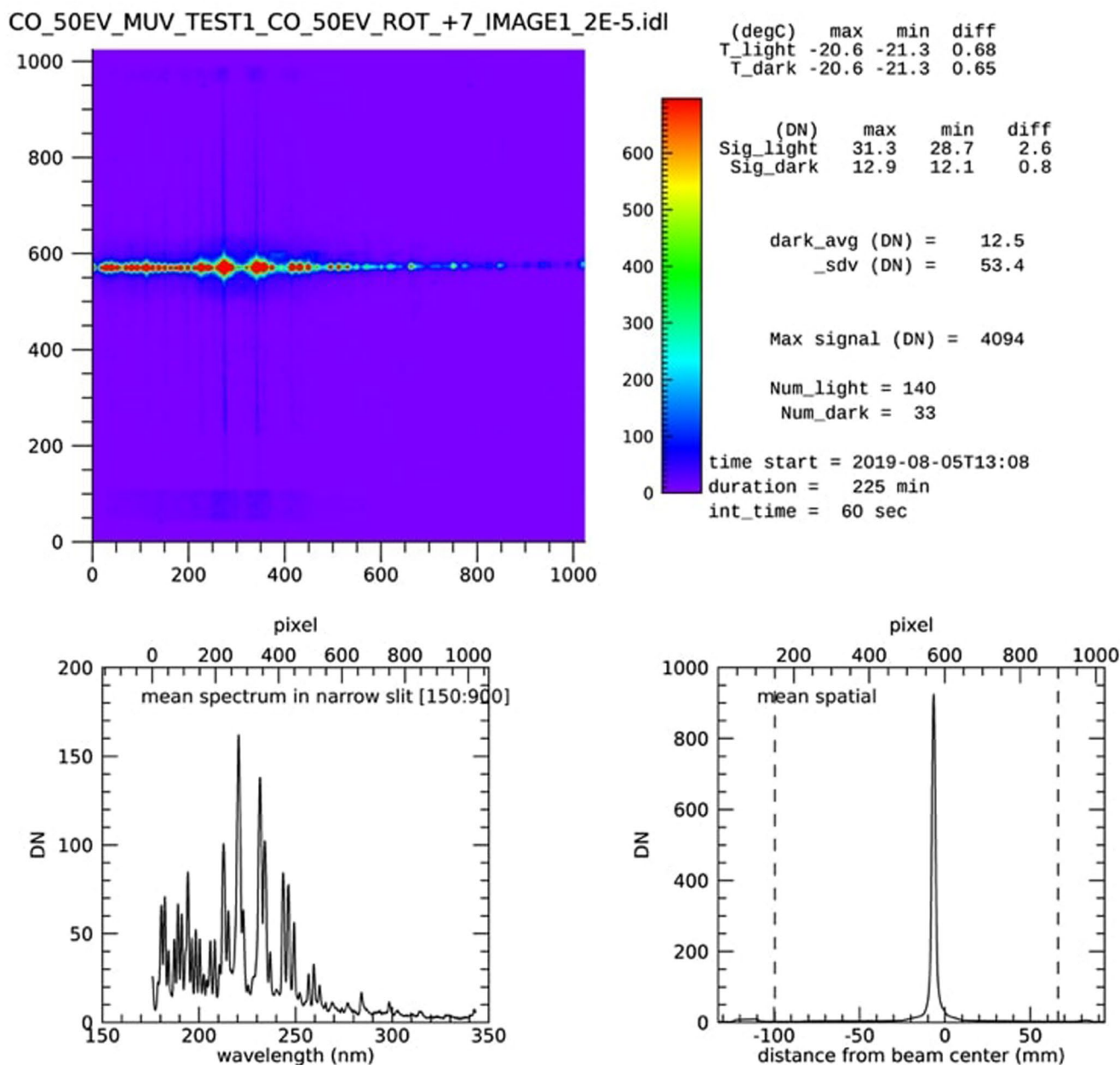


Figure 2. Details of the IUVS MUV imaging channels: (Upper left) Image-1 file of e + CO (50 eV) measurements showing $1,024 \times 1,024$ spatial and spectral pixels. The image is formed from electron impact direct excitation of CO. The spectrum is highlighted in the MUV by CBs, 1NG, and 4PG. We use spatial pixels 150:900, where the effects of internal scattering for the narrow slit is minimized. The broad occultation slit at the top of the IUVS extends from spatial pixels 50:150 in the image, and the smaller occultation slit at the bottom extends from spatial pixel 950:1000 and views the region above the electron beam as the IUVS moves vertically upward. (Upper right) Engineering readouts detector temperature ($^{\circ}\text{C}$) and minimum and maximum signal (counts per minute) variations observed during the measurement. The Point-Spread Function (PSF) measurement had a duration of 220 min, with 60 s integrations. (Bottom left) Mean spectrum in narrow slit averaged over spatial pixels 150:900. (Bottom right) Mean spatial intensity with distance from electron beam.

OEU mounted to a vertically moving stage, to fully observe and measure optically allowed and forbidden transitions. Each spatial pixel spans an object region of 0.220 mm. The MUV spectral image was obtained in first spectral order by the IUVS OEU yielding about 0.16 nm per channel with a measured spectral resolution of ~ 1.2 nm full width at half maximum (FWHM) in the plane of dispersion (Figure 2).

Long-exposure spectra (2–10 h) were taken with the IUVS OEU detector at positions $z = 0, 15.24$, and 30.48 cm above the electron beam axis (referred to as images 1, 2, and 3, respectively). The concatenation of

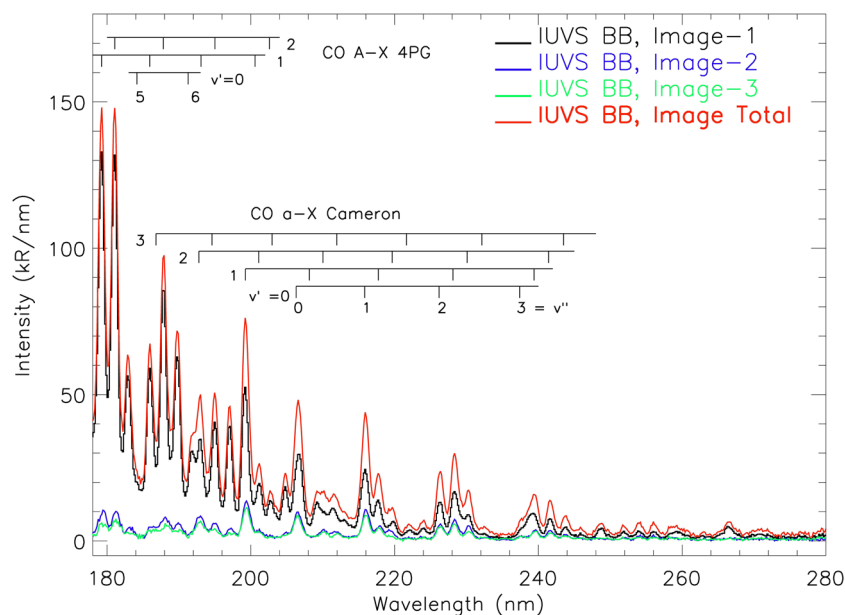


Figure 3. Calibrated MUV electron-impact-induced fluorescence spectrum of $e + \text{CO}$ from 180 to 280 nm with CB identifications. The data show four sets of experimental spectra for the three image positions as well as the sum of the three images at 30 eV. Image-1, Image-2, and Image-3 were taken with the IUVS-OEU optical axis vertically raised with respect to the electron beam at 0, 15.2, and 30.4 cm, respectively.

these images produces the full spectrum (total image; Figure 3). The spectra were calibrated to the flight-instrument sensitivity (see Section 4.1) for use in emission cross section (Figures 6 and 7) and a $^3\Pi$ state lifetime (Figure 8) calculations.

4. Spectral Analysis

4.1. The Point-Spread Function and MUV Sensitivity Calibration

An important diagnostic of the “breadboard” IUVS OEU optical performance in the laboratory requires a measurement of the PSF. The PSF of the OEU was measured to be 0.47 nm FWHM in second order in the FUV, and the MUV OEU sensitivity calibration was found to be identical to the flight instrument. The PSF used in the present analysis is described in Equation 5 and Figure 2 of Ajello et al. (2019). The IUVS OEU responsivity was measured in the 190–300 nm range using a deuterium lamp, which had a calibration traceable to NIST (Saunders et al., 1978), as a standard irradiance source. The lamp illuminated a Spectralon® diffuse calibrated Lambertian reflectance surface, which was placed ~ 1 m from the instrument entrance pupil providing a calibrated radiance target. The output of the instrument in data numbers (DN) was divided by the screen radiance to provide spectrally dependent radiance coefficients ([DN/photons/cm²/sr/s]). Self-absorption, which is significant for wavelengths less than 250 nm, was estimated and removed by comparing spectra that were measured at a lamp-to-screen distance of 56 cm to those at a distance of 112 cm.

The IUVS OEU calibration coefficients were compared to those of the flight MAVEN IUVS instrument obtained using the same lamp, screen, and illumination geometry. These agreed within $\pm 10\%$ over the entire 190–300 nm wavelength range. Based on these results, we used the flight instrument coefficients to extend the engineering model calibration to the 170–190 nm range. After launch, the flight instrument responsivity in the range 170–240 nm was increased based on observations of stars during cruise to Mars (Deighan et al., 2015). This update was applied to the engineering model responsivity for this work as well.

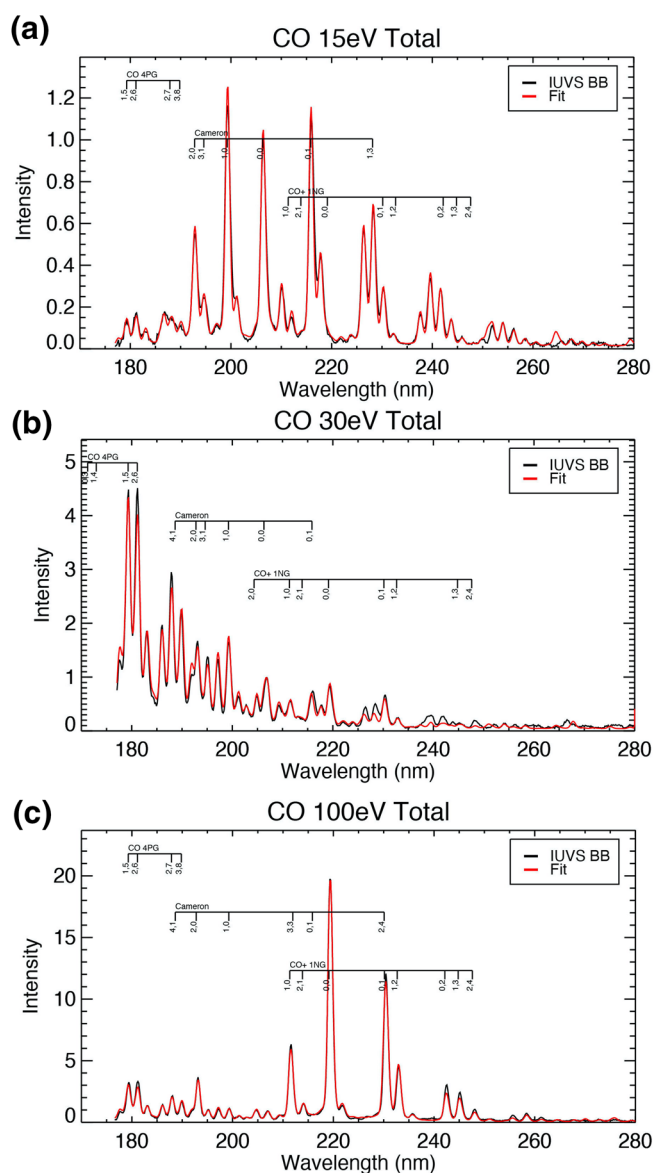


Figure 4. Measured electron-impact-fluorescence MUV spectra (black) from a CO gas for (a) 15 eV, (b) 30 eV, and (c) 100 eV electrons compared with MLR fits (red) from 4PG, 1 NG, and CB model vectors shown in Figure 5.

4.2. MUV Electron Impact Spectra of CO

We have studied the electron-impact-fluorescence MUV spectra of CO with the IUVS OEU instrument from 180 to 280 nm in a large vacuum chamber as described in Ajello et al. (2017). The calibrated spectra for each of the three images, as well as the summed total spectrum, are shown in Figure 3 for CO from electron impact fluorescence at 30 eV. To our knowledge, these are the first MUV spectra of CO with a large enough chamber to fully sample dipole-allowed and optically forbidden emissions and to account for a small loss of CO($a^3\Pi$) excited molecules to the walls. The wavelength range for the strong observed CB system is 180–280 nm, and the vibrational level tick marks of the CB are depicted in detail. The previously published MUV uncalibrated electron impact spectra of CO at 20 and 50 eV, obtained in a small vacuum chamber with a small FOV, were pictorially shown in the work of Ajello (1971a, 1971b) and were analytically intercompared after calibration for cross section analysis. The 4PG CO($A^1\Pi \rightarrow X^1\Sigma^+$), the 1NG CO($B^2\Sigma^+ \rightarrow X^2\Sigma^+$), and the CB CO($a^3\Pi \rightarrow X^1\Sigma^+$) are the band systems of CO and CO $^+$ observed in Figure 3, which are also excited by CO $_2$ dissociative excitation.

The 4PG system has been discussed extensively in a previous paper about the FUV (Ajello et al., 2019). For the 1NG system of CO $^+$ ($B^2\Sigma^+ \rightarrow X^2\Sigma^+$) which extends from 180 to 320 nm, there are no upper electronic levels that cascade to the $B^2\Sigma^+$ state, which has a threshold at 19.66 eV. The peak cross section occurs at 150 eV and has a value of $4.30 \times 10^{-17} \text{ cm}^2$ (Ajello, 1971a, 1971b). The excitation function for the 1NG is described in Ajello (1971a, 1971b). For the 1NG CO $^+$ ($B^2\Sigma^+ \rightarrow X^2\Sigma^+$), an electronic transition where the change in internuclear distance is small, the band system is confined to a small wavelength range. In fact, no 1NG bands for $v' > 3$ were observed. The entire 1NG spectrum was confined to an interval from 205 to 260 nm and is clearly evident as overlapping the CB shown in Figures 4c and 5c at 100 eV.

The CB are of primary interest in this study as the only forbidden feature observed in the MUV for electron-impact on CO. The 15 eV MUV spectrum is shown in Figures 4a and 5a. The measured and theoretical Franck-Condon factors (FCFs) $q_{v'}$ for excitation to vibrational level v' from $v'' = 0$ (Table 1; Meléndez et al., 2002) do not agree due to significant cascading from the $d^3\Delta$ and $a'^3\Sigma^+$ electronic states to the a-state from both these strong triplet states and both with internuclear minima well separated from the a-state as shown in Figure 1. Cascading will preferentially excite a wide range from 5 to 10 of high v' vibrational levels of the $d^3\Delta$ and $a'^3\Sigma^+$ electronic states and will excite a wide range of a-state vibrational levels by cascading leading to a peak v' in the range of $v' = 1$ –3

as shown in Krupenie (1966). The excitation cross section, $\sigma_{v'}$, is strongly dependent on vibrational level with a peak at $v' = 1$ (Conway, 1981). Thus for $v' > 3$ one would not expect any measurable radiation since the fraction of the total excitation cross section represented by levels with $v' > 3$ is less than 1% but with cascading there is excitation of the a-state to $v' = 7$ (Ajello, 1971a, 1971b). Ajello et al. (2019) and references therein (Krupenie, 1966; Morton & Noreau, 1994; Tilford & Simmons, 1972) have also shown there is strong coupling between the CO($A^1\Pi$) \sim CO($a^3\Pi$) states from single-triplet perturbations. Figure 3 shows the contribution to the total emission cross section by the cascade emissions from images 2 and 3 imaging the glow at ~ 15 and ~ 30 cm, respectively, from the excitation source. Together these contributions account for $\sim 55\%$ of the total CB emission cross section at 20 eV (further discussed in Section 4.3).

Individual molecular rotational and atomic multiplets were spectrally smeared using the PSF (Equation 5 and Figure 2 from Ajello et al. [2019]) to model the measured electron-impact-fluorescence MUV spectra

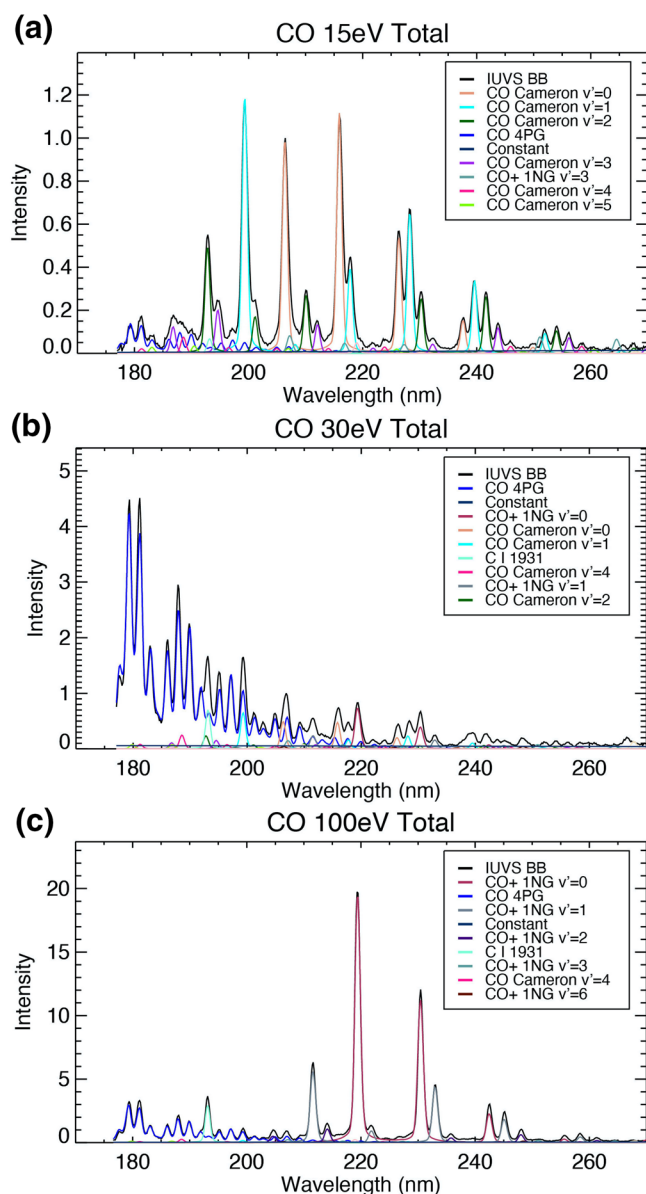


Figure 5. Measured electron-impact-fluorescence MUV spectra (black) from a CO gas for (a) 15 eV, (b) 30 eV, and (c) 100 eV electrons compared with an optically thin MLR fit using 4PG, 1NG, and CB vectors.

from CO gas as shown in Figure 5. These modeled sources, along with a linear background, were then put into a constrained MLR fit of each source intensity to the measured spectra. Each source was treated as a free parameter and constrained with the requirement that fit coefficients be nonnegative. Molecular sources were modeled using AURIC rovibrational band models for CB, 4PG, and 1NG (Ajello et al., 2019; Stevens et al., 2015). The rotational temperature used for the three band models was 300 K. Comparisons of the measured electron-impact-fluorescence CO total spectra (black) with the MLR best fit (red) are shown in Figures 4a, 4b, and 4c for 15, 30, and 100 eV, respectively. The dominant sources determined from the fits to the measured spectra in Figure 4 are shown in Figures 5a, 5b, and 5c for 15, 30, and 100 eV, respectively. The CB and 1NG models used to fit the spectra in Figure 4 are separated into upper levels (v') and the upper level vibrational populations are retrieved directly from the measured spectra. For the 4PG band model, we assume the vibrational populations reported by Ajello et al. (2019). The MLR best fit CB and 1NG populations are shown in Tables 1 and 2, along with FCFs for $v'' = 0$ reported by Meléndez et al. (2002) and Szajna et al. (2004), respectively.

4.3. The Electronic Emission Cross Sections

We have measured the emission cross section of the CB in the MUV (180–280 nm) from the process $e + \text{CO}$, with a threshold for the $a^3\Pi$ state at 6.04 eV, at various electron impact energies: 15, 20, 40, 50, and 100 eV. The CB emission cross sections are shown in Table 3 and Figure 6 with comparison to previous measurements by Zetner et al. (1998) at low energy, and the experimental work of Furlong and Newell (1996), which are relative $\text{CO}(a^3\Pi)$ excitation cross sections normalized to the summed excitation cross sections of $\text{CO}(a^3\Pi, a'^3\Sigma^+, d^3\Delta)$ states at 15 eV from Table 2 of Zetner et al. (1998). There is significant population of the $a^3\Pi$ state formed by cascade from higher electronic levels which have an onset at 9.3 eV (Furlong & Newell, 1996). This emission cross section has not been accurately measured in any previous UV experiment due to insufficient mean-free-path allowance for the total MUV emission from the long-lived, optically forbidden, spin-forbidden transitions occurring far from the electron-impact source. In this experiment, with a lifetime of 3 ms (Section 4.4) and a mean thermal energy of 39 MeV at 300 K, we can calculate the fraction of excited molecules observed inside the 400 mm of the observed glow cylinder with the formulation in Ajello et al. (2019).

The mean distance an excited $\text{CO}(a^3\Pi)$ molecule will travel once excited on the axis of the electron gun is 1,560 mm. The $1/r$ fall off of intensity, together with an exponential decrease depending on lifetime, shows that the IUVS captures 62% of the radiation with 38% of excited molecules deactivated at the walls of the experimental chamber. A correction factor of 38% is applied to the $\text{CO}(a^3\Pi)$ CB intensity when compared to the prompt $\text{CO}(A^1\Pi \rightarrow X^1\Sigma^+)$ 4PG emission longward of 180 nm. Based on our study of the 4PG cross section as a function of energy (Ajello et al., 2019), we find the fraction of the 4PG emission cross section above 180 nm is 12.3%, leading to an emission cross section of the 4PG system in the wavelength range 180–280 nm of $5.8 \times 10^{-18} \text{ cm}^2$ at 15 eV. A similar approach is used for other electron energies. This method then provides absolute cross section standard values for measurement of CB and 1NG cross sections in the MUV in this experiment. Specifically, MLR fits to MUV data for each electron energy are constructed as described in Section 4.2 to determine relative contributions for each source of emission (4PG, CB, 1NG, atomic multiplets, background; see Figure 4). Taking the ratios of integrated CB or

Table 1
CO Cameron Population Fits at 15 eV Normalized to Unity, Along With the FCFs ($v'' = 0$) From Table 6 of Meléndez et al. (2002)

v'	This work	Meléndez et al. (2002)
0	0.328	0.268
1	0.341	0.313
2	0.195	0.218
3	0.084	0.116
4	0.032	
5	0.012	
6	0.004	
7	0.002	

Table 2
CO⁺ 1NG Population (at 40 eV Fits Normalized to Unity, Shown With the FCFs ($v'' = 0$) From Szajna et al. (2004)

v'	This work	Szajna et al. (2004)
0	0.409	0.538
1	0.290	0.315
2	0.202	0.109
3	0.074	0.029
4	0.022	0.007
5	0.003	0.002

Table 3
Cameron Band Total Emission Cross Sections From Electron Impact of CO From 180 to 280 nm With an Uncertainty of 35% (Ajello et al., 2020)

Energy (eV)	σ_{em} (10^{-18} cm ²) ^a	$\sigma_{ex}(a^3\Pi)^b$	$\sigma_{ex}(a'^3\Sigma^+)^b$	$\sigma_{ex}(d^3\Delta)^b$	Total σ_{ex} EELS
15	76.5	28.5	13.1	32.0	73.6
20	15.6	—	—	—	—
40	4.8	—	—	—	—
50	5.8	—	—	—	—
100	7.7	—	—	—	—

Note. For comparison with previous CB cross section measurements, see Figure 6.

^aThis work. ^bZetner et al. (1998).

1NG sources to the blended 4PG source allows for propagating the MUV 4PG standard cross section values for each electron energy to calculate corresponding CB and 1NG cross sections. The 1NG cross sections are given in Table 4 and are compared to previous measurements averaged in Avakyan et al. (1998).

The unique experimental facility employed here—a large vacuum chamber with imaging capabilities in the vacuum ultraviolet—is ideal (and necessary) for the emission measurements presented in Table 3. For example, the emission cross section at 15 eV in Table 3 is complicated by significant cascade emissions. We demonstrate this effect in Table 3 by comparing the 15 eV emission cross section measured in this work to the individual excitation cross sections measured by Zetner et al. (1998). The major contributor to the CO ($a^3\Pi \rightarrow X^1\Sigma^+$) emission cross section near the peak at 10–15 eV is the cascading transition $d^3\Pi \rightarrow a^3\Pi$, with a cascade cross section of 3.2×10^{-17} cm² at 15 eV compared to 2.85×10^{-17} cm² for the CO($X^1\Sigma^+ \rightarrow a^3\Pi$) direct excitation cross section at 15 eV of Zetner et al. (1998).

As shown in Table 3, cascade effects provide half the UV emission cross section. Compare our result to the individual and summed excitation cross sections of Zetner et al. (1998). The higher CO states that cascade down to the CO $a^3\Pi$ arise from the transitions $d^3\Delta \rightarrow a^3\Pi$ (triplet bands) and $a'^3\Sigma^+ \rightarrow a^3\Pi$ (Asundi bands) that are fully allowed transitions (Judge & Lee, 1973; L. C. Lee and Judge, 1973). To a small extent, the $e^3\Sigma^-$ state also contributes to cascading. Emission from these higher cascading CO states, found in the visible spectral region, are cumulatively as intense as the Cameron band emission produced from direct excitation. We also show in Figure 6, the summary of excitation cross sections CO($X^1\Sigma^+ \rightarrow a^3\Pi$) from threshold to 71.09 eV from Table 1 of Furlong and Newell (1996) normalized at 15 eV to the summed total direct excitation cross section of Zetner et al. (1998) for CO($a^3\Pi$, $a'^3\Sigma^+$, $d^3\Delta$) states from their Table 2. The emission cross section of the CB from our work are compared to the excitation + cascade cross section metastable time of flight normalized measurements of Furlong and Newell (1996), and to the published high resolution measurements of Zetner et al. (1998) who clearly resolved the triplet states of direct and cascade excitation to the $a^3\Pi$. The summed total direct cross section value of Zetner et al. (1998) is 7.4×10^{-17} cm² at 15 eV. Our emission cross section value at 15 eV is 7.7×10^{-17} cm². This close agreement is shown in Figure 6 and indicates a peak emission cross section of 1.1×10^{-16} cm² at 10 eV.

We show in Figure 7 the compilation of our results for the 1NG bands, the 4PG, and CB from our MUV work and list in Table 4 the new recommended cross sections for the CB and 1NG bands based on the cross section of the 4PG system above 180 nm, which is the absolute calibration standard used in this experiment (Ajello et al., 2019). Continuous cross

section curves over energy were analytically fit to the calculated values with a general, unbound MLR according to the formulation in Appendix A of Yonker and Bailey (2020). The coefficients used for the analytic fit are given in Table 5.

4.4. Lifetime of the CO ($a^3\Pi$) State From Analysis of the Cameron Band Glow Profile

The distance a CO ($a^3\Pi$) molecule will travel before radiating depends on its lifetime. The distance that a CO ($a^3\Pi$) molecule will travel also depends on the mean thermal energy of 39 meV at 300 K

Table 4
First Negative and Fourth Positive Group Emission Cross Sections With an Uncertainty of 30% From Electron Impact of CO

Energy (eV)	σ_{em} 1NG (10^{-18} cm ²)		σ_{em} 4PG (10^{-18} cm ²)
	This work	Avakyan et al. (1998)	Ajello et al. (2019) 180–280 nm
15	–	–	5.8
20	0.2	0.13	6.8
40	5.9	7.3	5.8
50	7.0	9.5	5.2
100	12.6	12.6	3.6

Note. The 1NG cross sections reported by Avakyan et al. (1998) are given for comparison. The 4PG cross section from 180 to 280 nm is the absolute cross section standard value used to measure the other cross sections.

laboratory temperature. The CB volume emission rate in the cylindrical glow about the electron beam falls off a little faster than $1/r$ due to the exponential factor with lifetime. The triplet states above the a-state in Figure 1 all radiate promptly to the $a^3\Pi$ state with a lifetime of the order of a few microseconds (Strobl & Vidal, 1987). We have shown that a measurement of the glow profile at room temperature is a measure of the lifetime (Ajello et al., 2017, 2019). The extent of the glow is larger with a longer lifetime or the higher the mean thermal velocity.

To reiterate, with staged three-step motion of the IUVS-OEU optical axis, the image plane (1,024×1,024 pixels; Figure 2) FOV measured by this three-step motion was expanded from –100 mm below to more than 400 mm above the electron beam axis allowing the observation of metastable CB emissions. Figure 8a shows the full glow concatenated pattern of the CB from 180 to 280 nm at 30 eV for the three images staged across the 0.75 m radius of MOBI from electron impact

fluorescence over the range of CO ($a^3\Pi$ state) lifetimes from 0.1 to 10 ms. We can model the Cameron glow as a function of minimum ray height radius to the line of sight. The model in Figure 8a indicates a best fit for a lifetime of 3 ms.

We show in Figure 8b a second model for an infinite cylinder not limited to a 400 mm minimum ray height. The two sets of glow models are composed of two spatial arrays to account for the CO ($a^3\Pi$) excited molecules that collide with the walls. The difference between a finite chamber of 0.75 m radius and a 5 m chamber amounts to only 6% loss along the line of sight as shown in the figure with a slower fall-off with distance. We account for this loss of signal in our cross section calculations. The best fit model for the direct excitation lifetimes in either case is 3 ms with an uncertainty of 1 ms. Thus, the CO ($a^3\Pi$) lifetime is 3 ± 1 ms.

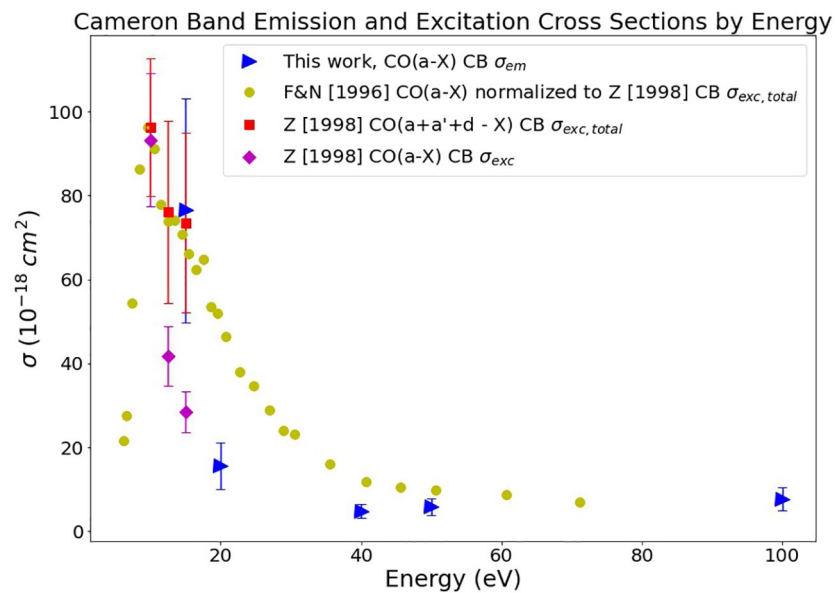


Figure 6. Cameron band CO ($a^3\Pi \rightarrow X^1\Sigma^+$) emission cross sections as a function of energy. We show a comparison of the emission function of this experiment (blue triangles) to the excitation cross section measurements of Zetner et al. (1998), both the excitation cross sections to the $a^3\Pi$ state (pink triangles) and the sum of excitation cross sections of the triplet states: $d^3\Delta + a^3\Pi + a'^3\Sigma^+$, (red squares; equivalently their best-estimate total emission cross section values of cascade + direct excitation). The cascade + excitation cross sections (gold circles) of Furlong and Newell (1996) in their Table 1 normalized at 15 eV to work of Zetner et al. (1998) are also shown for comparison.

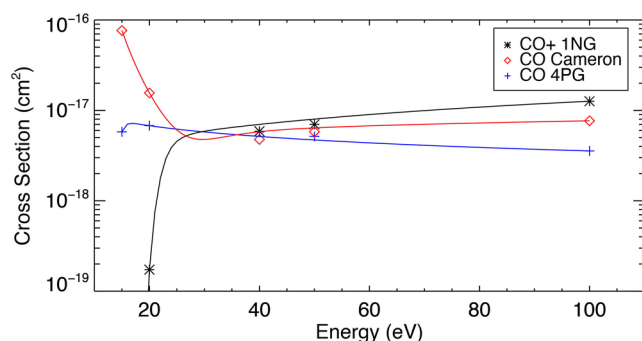


Figure 7. 4PG, 1NG, and Cameron Band cross sections as a measured in this work as a function of energy. Data points represent the measured cross sections from this study, and intermediate values were interpolated using the analytic fit formulation described in Yonker and Bailey (2020). The coefficients used in this fit are given in Table 5.

Past measurements include work by Borst and Zipf (1971), who found the average lifetime of metastable CO molecules in the $a^3\Pi$ state excited by electron impact at 7.5 eV at room temperature to be about 1 ms. More recently, Gilijamse et al. (2007) have studied the phosphorescence decay of the $a^3\Pi v = 0, J = 1$ level, and found a radiative lifetime of 2.63 ms.

5. Summary and Conclusions

UV missions to Mars by NASA, ESA, and other space agencies have been motivated by observations of UV dayglow that responds to solar cycle EUV variation, which over eons determines the escape of gases (H and O) in Mars' volatile evolution. A brief review of the history of $e + CO$ CB emission spectral measurements reveals the necessity of a correction to the emission and excitation cross sections through experimentation in a sufficiently large vacuum chamber. Previous emission cross section uncertainties propagate error into aeronomical analyses of Martian dayglow. We have obtained $e + CO$ spectra at 15, 20, 40, 50, and 100 eV to

refine electron transport models of CB. New recommendations for emission cross sections of the CB and the 1NG are presented (Tables 3 and 4), as well as a lifetime estimate of the metastable $CO(a^3\Pi)$ state of 3 ± 1 ms (Figure 8). Currently in common use are the values from Erdman and Zipf (1983) with varying scaling factors applied. Determining these cross sections establishes an improved set of fundamental physical constants for electron impact codes to be used in the accurate analysis of UV spectra in current and future missions to Mars, Venus, and other planetary bodies. A thorough understanding of these important emissions in determining atmospheric escape may leverage discoveries about ionospheric activity throughout our solar system and beyond.

The knowledge of the energy dependence of the electron impact cross section on CO and CO_2 is essential for the interpretation of the CO CB in terms of the composition of Mars and Venus' upper atmospheres. Models indicate that a major source of excitation of the CO ($a^3\Pi$) state near the peak in the dayglow and aurora is electron impact on CO_2 (Bhardwaj & Jain, 2013; Gérard et al., 2019; Leblanc et al., 2006). However, there has been recent evidence that electron impact on CO may also play an important role on Mars in the production of the CB above the emission peak (González-Galindo et al., 2018, 2019). A consequence is that the Cameron emission scale height may be significantly larger than the CO_2 scale height and that the use of the topside scale height of CB limb profile to determine the temperature is not straightforward. Comparisons of the scale heights of the CB and the CO_2^+ UV doublet (González-Galindo et al., 2019) confirm that indeed the latter is generally smaller than the former. Conversely, at high altitude, the intensity of the CB can be a useful tool to determine the CO density. The CO density is a quantity difficult to determine by other methods. For example, neutral gas and ion mass spectrometer measurements of CO from MAVEN can be made down to 130 km only occasionally during “deep dip phases” (Mahaffy et al., 2015). CO density determination from the Cameron dayglow is possible only if the cross section for the main source of excitation (electron impact on CO in this case) and its energy dependence are accurately known. The measurements reported in this study fill this gap and open a new possibility to map the CO density distribution.

Table 5

Coefficients (c_i) Used to Determine Analytic Fit to Emission Cross Sections in c_i are Determined Using the Formulation in Appendix A of Yonker and Bailey (2020)

		Coefficients							
	Threshold energy (eV)	c_1	c_2	c_3	c_4	c_5	c_6	c_7	c_8
CB	5.56	4.83	0.24	24.80	−5.93	19.21	−3.78	1.00	−1.21
1NG	18.38	3.25	−0.37	4.81	−3.26	3.17	0.69	4.86	−3.28
4PG	12.67	2.21	−0.56	2.20	−3.76	5.73	−0.36	7.00	−0.74

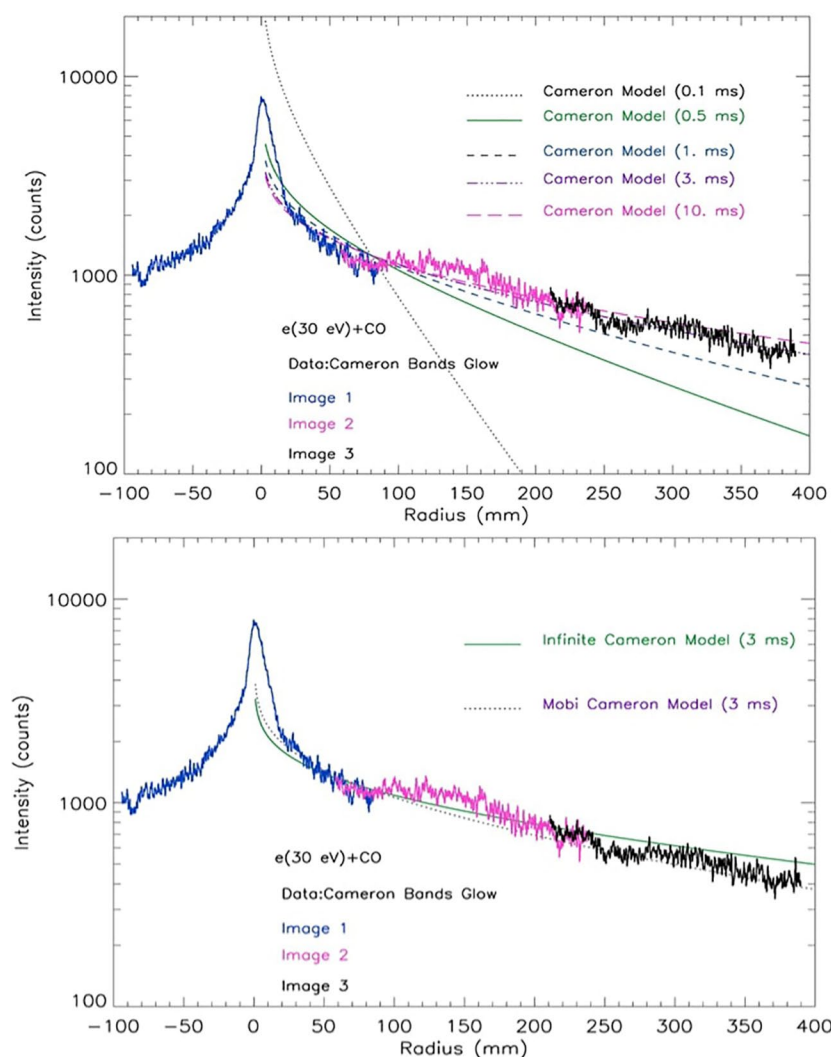


Figure 8. The radial glow functions of the CB (180–280 nm) from electron excitation of CO for Image-1, Image-2, and Image-3. The three images are concatenated and overlapped at the extremes of each image step to establish the 0–400 mm glow pattern from electron beam to chamber wall shroud. Included in the figure are modeled glow patterns for the CB source with a range of lifetimes from 0.1 to 10 ms lifetime at 300 K with mean thermal kinetic energy 39 meV.

The CO mixing in both the Mars and Venus thermospheres is expected to be variable since it is submitted redistribution by the global circulation following CO₂ dissociation (Jain et al., 2015). Therefore, spatial variations in the spectral distribution of the CB in the upper thermosphere could be an indicator of seasonal, latitudinal, or local time changes in the CO/CO₂ mixing ratio. Similarly, detailed comparisons between the CB structure on Mars and Venus would reveal differences in chemical composition. Future comparisons of the spectral distribution of the CB dayglow and aurora in Mars and Venus with the e + CO and e + CO₂ laboratory spectra will make it possible to assess the contribution of CO to the a ³Π state production.

Data Availability Statement

Data used are cited in the references. Original laboratory data used in these analyses are publicly available (R. Lee and Ajello, 2020). Data reduction and analysis scripts are available on Zenodo (Holsclaw, 2020; Veibell, 2020).

Acknowledgments

This work was primarily performed at the Laboratory for Atmospheric and Space Physics (LASP), University of Colorado (CU) Boulder, and the Jet Propulsion Laboratory (JPL), California Institute of Technology (Caltech), under a contract with the National Aeronautics and Space Administration (NASA). We gratefully acknowledge financial support through NASA's Solar System Workings (SSW), Cassini Data Analysis Program (CDAP), the Helio-physics H-TIDEs and Geospace Science programs, Mars Data Analysis Program (MDAP), and the National Science Foundation (NSF) GEO-AGS Aeronomy program. J.-C. Gérard is supported by the PRODEX program managed by the European Space Agency (ESA) with help from the Belgian Federal Science Policy Office (BELSPO). R. A. Lee thanks the NSF Research Experience for Undergraduates (REU) program for support. We thank X. Liu for 4PG rovibrational spectral models. We thank Karl Hubbell for technical support and Bruce Jakosky, and the MAVEN team, for usage of the IUVS optical-engineering unit (OEU). U.S. government sponsorship is acknowledged.

References

- Ajello, J. M. (1971a). Emission cross sections of CO by electron impact in the interval 1260–5000. *The Journal of Chemical Physics*, 55, 3158–3168. <https://doi.org/10.1063/1.1676563>
- Ajello, J. M. (1971b). Emission cross sections of CO₂ by electron impact in the interval 1260–5000. *The Journal of Chemical Physics*, 55, 3169–3177. <https://doi.org/10.1063/1.1676564>
- Ajello, J. M., Evans, J. S., Veibell, V., Malone, C. P., Holsclaw, G. M., Hoskins, A. C., et al. (2020). The UV spectrum of the Lyman-Birge-Hopfield band system of N₂ induced by cascading from electron impact. *Journal of Geophysical Research: Space Physics*, 125, e2019JA027546. <https://doi.org/10.1029/2019JA027546>
- Ajello, J. M., Malone, C. P., Evans, J. S., Holsclaw, G. M., Hoskins, A. C., Jain, S. K., et al. (2019). UV study of the fourth positive band system of CO and O | 135.6 nm from electron impact on CO and CO₂. *Journal of Geophysical Research: Space Physics*, 124, 2954–2977. <https://doi.org/10.1029/2018JA026308>
- Ajello, J. M., Malone, C. P., McClintock, W. E., Hoskins, A. C., & Eastes, R. W. (2017). Electron impact measurement of the 100 eV emission cross section and lifetime of the Lyman-Birge-Hopfield band system of N₂: Direct excitation and cascading. *Journal of Geophysical Research: Space Physics*, 122(6), 6776–6790. <https://doi.org/10.1002/2017JA024087>
- Al Matroushi, H., Lootah, F., Holsclaw, G., Deighan, J., Chaffin, M., EMUS, team, et al. (2019). Scientific payload of the Emirates Mars Mission: Emirates Mars Ultraviolet Spectrometer (EMUS) overview. Ninth International Conference on Mars LPI Contribution No. 2089, id. 6073 Pasadena, CA. Retrieved from <https://ui.adsabs.harvard.edu/abs/2019LPLC02089.6073A>
- Avakyan, S. V., Il'in, R. N., Lavrov, V. M., & Ogurtsov, G. N. (1998). *Collision processes and excitation of UV emission from planetary atmospheric gases: A handbook of cross sections*. India: Gordon and Breach Science Publishers.
- Barth, C. A., Hord, C. W., Pearce, J. B., Kelly, K. K., Anderson, G. P., & Stewart, A. I. (1971). Mariner 6 and 7 ultraviolet spectrometer experiment: Upper atmosphere data. *Journal of Geophysical Research*, 76(10), 2213–2532. <https://doi.org/10.1029/JA076i010p02213>
- Barth, C. A., Hord, C. W., Stewart, A. I., Lane, A. L., Dick, M. L., & Anderson, G. P. (1973). Mariner 9 ultraviolet spectrometer experiment: Seasonal variation of ozone on Mars. *Science*, 179, 795–796. <https://doi.org/10.1126/science.179.4075.795>
- Barth, C. A., Stewart, A. I., Hord, C. W., & Lane, A. L. (1972). Mariner 9 ultraviolet spectrometer experiment: Mars airglow spectroscopy and variations in Lyman alpha. *Icarus*, 17, 457–462. [https://doi.org/10.1016/0019-1035\(72\)90011-5](https://doi.org/10.1016/0019-1035(72)90011-5)
- Bertaux, J.-L., Korabev, O., Perrier, S., Quémarais, E., Montmessin, F., Leblanc, F., et al. (2006). SPICAM on Mars Express: Observing modes and overview of UV spectrometer data and scientific results. *Journal of Geophysical Research*, 111, E10S90. <https://doi.org/10.1029/2006JE002690>
- Bhardwaj, A., & Jain, S. K. (2013). CO Cameron band and UV doublet emissions in the dayglow of Venus: Role of CO in the Cameron band production. *Journal of Geophysical Research: Space Physics*, 118(6), 3660–3671. <https://doi.org/10.1002/jgra.50345>
- Borst, W. L., & Zipf, E. C. (1971). Lifetimes of metastable CO and N₂ molecules. *Physical Review A*, 3(3), 979–989. <https://doi.org/10.1103/PhysRevA.3.979>
- Chaufray, J.-Y., Bertaux, J.-L., & Leblanc, F. (2012). First observation of the Venus UV dayglow at limb from SPICAV/VEX. *Geophysical Research Letters*, 39(20), L20201. <https://doi.org/10.1029/2012GL053626>
- Conway, R. R. (1981). Spectroscopy of the Cameron bands in the Mars Airglow. *Journal of Geophysical Research*, 86(A6), 4767–4775. <https://doi.org/10.1029/JA086iA06p04767>
- Deighan, J., Chaffin, M. S., Chaufray, J.-Y., Stewart, A. I. F., Schneider, N. M., Jain, S. K., et al. (2015). MAVEN IUVS observation of the hot oxygen corona at Mars. *Geophysical Research Letters*, 42(21), 9009–9014. <https://doi.org/10.1002/2015GL065487>
- Erdman, P. W., & Zipf, E. C. (1983). Electron-impact excitation of the Cameron system (a ³Π → X¹Σ) of CO. *Planetary and Space Science*, 31(3), 317–321. [https://doi.org/10.1016/0032-0633\(83\)90082-X](https://doi.org/10.1016/0032-0633(83)90082-X)
- Evans, J. S., Stevens, M. H., Lumpe, J. D., Schneider, N. M., Stewart, A. I. F., Deighan, J., et al. (2015). Retrieval of CO₂ and N₂ in the Martian atmosphere using dayglow observations by IUVS on MAVEN. *Geophysical Research Letters*, 42(21), 9345–9589. <https://doi.org/10.1002/2015GL065489>
- Feldman, P. D., Burgh, E. B., Durrance, S. T., & Davidsen, A. F. (2000). Far-ultraviolet spectroscopy of Venus and Mars at 4 Å resolution with the Hopkins ultraviolet telescope on Astro-2. *The Astrophysical Journal*, 538(1), 395–400. <https://doi.org/10.1086/309125>
- Ferlet, R., André, M., Hébrard, G., Lecavelier des Etangs, A., Lemoine, M., Pineau des Forêts, G., et al. (2000). Far ultraviolet spectroscopic Explorer observations of the HD molecule toward HD 73882. *The Astrophysical Journal*, 538(1), L69–L72. <https://doi.org/10.1086/312799>
- Fox, J. L. (2008). Morphology of the dayside ionosphere of Venus: Implications for ion outflows. *Journal of Geophysical Research*, 113, E11001. <https://doi.org/10.1029/2008JE003182>
- Furlong, J. M., & Newell, W. R. (1996). Total cross section measurement for the metastable a ³Π state in CO. *Journal of Physics B: Atomic, Molecular and Optical Physics*, 29, 331–338. <https://doi.org/10.1088/0953-4075/29/2/020>
- Gérard, J. C., Bougher, S. W., López-Valverde, M. A., Pätzold, M., Drossart, P., & Piccioni, G. (2017). Aeronomy of the Venus upper atmosphere. *Space Science Reviews*, 212, 1617–1683. <https://doi.org/10.1007/s11214-017-0422-0>
- Gérard, J. C., Gkouvelis, L., Ritter, B., Hubert, B., Jain, S. K., & Schneider, N. M. (2019). MAVEN-IUVS observations of the CO₂⁺ UV doublet and CO Cameron bands in the Martian thermosphere: Aeronomy, seasonal, and latitudinal distribution. *Journal of Geophysical Research: Space Physics*, 124, 5816–5827. <https://doi.org/10.1029/2019JA026596>
- Gérard, J. C., Hubert, B., Gustin, J., Shematovich, V., Bisikalo, D. V., Gladstone, G. R., & Esposito, L. W. (2011). EUV spectroscopy of the Venus EUV dayglow with UVIS on Cassini. *Icarus*, 211, 70–80. <https://doi.org/10.1016/j.icarus.2010.09.020>
- Gilijamse, J. J., Hoekstra, S., Meek, S. A., Metsäälä, M., van de Meerakker, S. Y. T., & Meijer, G. (2007). The radiative lifetime of metastable CO (a ³Π, v = 0). *The Journal of Chemical Physics*, 127(22), 221102. <https://doi.org/10.1063/1.2813888>
- González-Galindo, F., Chaufray, J. Y., Forget, F., García-Comas, M., Montmessin, F., Jain, S. K., & Stiepen, A. (2018). UV dayglow variability on Mars: Simulation with a global climate model and comparison with SPICAM/MEx data. *Journal of Geophysical Research: Planets*, 123(7), 1934–1952. <https://doi.org/10.1029/2018JE005556>
- González-Galindo, F., Jiménez-Monferrera, S., López-Valverde, M. A., García-Comas, M., & Forget, F. (2019). 'On the derivation of temperature from dayglow emissions on Mars' upper atmosphere. EPSC-DPS Joint Meeting 2019. Vol. 13. EPSC-DPS2019-888-1. Geneva: EPSC Abstracts, September 2019. Retrieved from <https://meetingorganizer.copernicus.org/EPSC-DPS2019/EPSC-DPS2019-888-1.pdf>
- Herzberg, G., Hugo, T. J., Tilford, S. G., & Simmons, J. D. (1970). Rotational analysis of the forbidden d ³Δ₁ ← X¹Σ⁺ absorption bands of carbon monoxide. *Canadian Journal of Physics*, 48(24), 3004–3015. <https://doi.org/10.1139/p70-373>
- Holsclaw, G. (2020). v1.0 Ajello-Lab/data_reduction: First release of Ajello-Lab data reduction IDL routine. [Data analysis scripts]. <https://doi.org/10.5281/zenodo.4270480>

- Hubert, B., Gérard, J.-C., Gustin, J., Shematovich, V. I., Bisikalo, D. V., Stewart, A. I., & Gladstone, G. R. (2010). UVIS observations of the FUV OI and CO 4P Venus dayglow during the Cassini flyby. *Icarus*, 207(2), 549–557. <https://doi.org/10.1016/j.icarus.2009.12.029>
- Huschilt, J., Dassen, H., & McConkey, J. (1981). Vacuum ultraviolet excitation of N_2 by low energy electrons: Polarization and excitation-function measurements. *Canadian Journal of Physics*, 59(12), 1893–1901. <https://doi.org/10.1139/p81-250>
- Itikawa, Y. (2002). Cross sections for electron collisions with carbon dioxide. *Journal of Physical and Chemical Reference Data*, 31(3), 749–767. <https://doi.org/10.1063/1.1481879>
- Itikawa, Y. (2015). Cross sections for electron collisions with carbon monoxide. *Journal of Physical and Chemical Reference Data*, 44(1), 03105. <https://doi.org/10.1063/1.4913926>
- Jain, S. K., Stewart, A. I. F., Schneider, N. M., Deighan, J., Evans, J. S., Stevens, M. H., et al. (2015). The structure and variability of Mars upper atmosphere as seen in MAVEN/IUVS dayglow observations. *Geophysical Research Letters*, 42(21), 9023–9030. <https://doi.org/10.1002/2015GL065419>
- Jakosky, B. M., Lin, R. P., Grebowsky, J. M., Luhmann, J. G., Mitchell, D. F., Beutelschies, G., et al. (2015). The Mars Atmosphere and Volatile Evolution (MAVEN) mission. *Space Science Reviews*, 195(1–4), 3–48. <https://doi.org/10.1007/s11214-015-0139-x>
- Judge, D. L., & Lee, L. C. (1973). Cross sections for the production of CO ($a' \ ^3\Sigma^+$, $d \ ^3\Delta_1$, and $e \ ^3\Sigma^- \rightarrow a \ ^3\Pi$) fluorescence through photodissociation of CO_2 . *The Journal of Chemical Physics*, 58(1), 104–107. <https://doi.org/10.1063/1.1678892>
- KanikNoren, I. C., Makarov, O. P., Vattipalle, P., Ajello, J. M., & Shemansky, D. E. (2003). Electron impact dissociative excitation of O_2 : 2. Absolute emission cross sections of OI(130.4 nm) and OI (135.6 nm) lines. *Journal of Geophysical Research*, 108(E11), 5126. <https://doi.org/10.1029/2000JE001423>
- Krasnopolsky, V. A., & Feldman, P. D. (2002). Far ultraviolet spectrum of Mars. *Icarus*, 160(1), 86–94. <https://doi.org/10.1006/icar.2002.6949>
- Krupenie, P. H. (1966). The band spectrum of carbon monoxide. National Standard Reference Data Series, Vol. 5. Washington, DC: NBS.
- Leblanc, F., Chaufray, J. Y., & Bertaux, J.-L. (2007). Martian dayglow as seen by the SPICAM UV spectrograph on Mars Express. *Geophysical Research Letters*, 34, L02206. <https://doi.org/10.1029/2006GL028437>
- Leblanc, F., Chaufray, J. Y., Lilensten, L., Witasse, O., & Bertaux, J. L. (2006). Martian dayglow as seen by the SPICAM UV spectrograph on Mars Express. *Journal of Geophysical Research*, 111, E09S11. <https://doi.org/10.1029/2005JE002664>
- Lee, R., & Ajello, J. (2020). Reduced MAVEN IUVS Breadboard data used for analyses in Lee et al. 2020 Laboratory Study of the Cameron Bands. *The first negative bands and fourth positive bands by electron impact on CO* [data set] Boulder, CO: University of Colorado. <https://doi.org/10.25810/M49V-G348>
- Lee, L. C., & Judge, D. L. (1973). Population distributions of triplet vibrational levels of CO produced by photodissociation of CO_2 . *Canadian Journal of Physics*, 51(4), 378–381. <https://doi.org/10.1139/p73-048>
- Mahaffy, P. R., Benna, M., Elrod, M., Yelle, R. V., Bougher, S. W., Stone, S. W., & Jakosky, B. M. (2015). Structure and composition of the neutral upper atmosphere of Mars from the MAVEN NGIMS investigation. *Geophysical Research Letters*, 42(21), 8951–8957. <https://doi.org/10.1002/2015GL065329>
- Makarov, O. P., Kanik, I., & Ajello, J. M. (2003). Electron impact dissociative excitation of O_2 : 1. Kinetic energy distributions of fast oxygen atoms. *Journal of Geophysical Research*, 108(E11), 5125. <https://doi.org/10.1029/2000JE001422>
- Malone, C. P., Johnson, P. V., McConkey, J. W., Ajello, J. M., & Kanik, I. (2008). Dissociative excitation of N_2O by electron impact. *Journal of Physics B: Atomic, Molecular and Optical Physics*, 41(9), 095201. <https://doi.org/10.1088/0953-4075/41/9/095201>
- McClintock, W. E., Schneider, N. M., Holsclaw, G. M., Clarke, J. T., Hoskins, A. C., Stewart, I., et al. (2015). The imaging ultraviolet spectrograph (IUVS) for the MAVEN mission. *Space Science Reviews*, 195(1–4), 75–124. <https://doi.org/10.1007/s11214-014-0098-7>
- Meléndez, F. J., Sandoval, L., & Palma, A. (2002). Franck–Condon factors for diatomic molecules with anharmonic corrections. *Journal of Molecular Structure: THEOCHEM*, 580(1–3), 91–99. [https://doi.org/10.1016/S0166-1280\(01\)00599-1](https://doi.org/10.1016/S0166-1280(01)00599-1)
- Morgan, L. A., & Tennyson, J. (1993). Electron impact excitation cross sections for CO. *Journal of Physics B: Atomic, Molecular and Optical Physics*, 26, 2429–2441. <https://doi.org/10.1088/0953-4075/26/15/026>
- Morton, D. C., & Noreau, L. (1994). A Compilation of Electronic Transitions in the CO Molecule and the Interpretation of Some Puzzling Interstellar Absorption Features. *The Astrophysical Journal Supplement Series*, 95, 301–343. <https://doi.org/10.1086/192100>
- Noren, C., Kanik, I., Ajello, J. M., McCartney, P., Makarov, O. P., McClintock, W. E., & Drake, V. A. (2001). Emission cross section of OI (135.6 nm) at 100 eV resulting from electron-impact dissociative excitation of O_2 . *Geophysical Research Letters*, 28(7), 1379–1382. <https://doi.org/10.1029/2000GL012577>
- Saunders, R. D., Ott, W. R., & Bridges, J. M. (1978). Spectral irradiance standard for the ultraviolet: The deuterium lamp. *Applied Optics*, 17(4), 593–600. <https://doi.org/10.1364/AO.17.000593>
- Shematovich, V. I., Bisikalo, D. V., Gérard, J.-C., Cox, C., Bougher, S. W., & Leblanc, F. (2008). Monte Carlo model of electron transport for the calculation of Mars dayglow emissions. *Journal of Geophysical Research*, 113(E2), E02011. <https://doi.org/10.1029/2007JE002938>
- Shematovich, V. I., Bisikalo, D. V., & Ionov, D. E. (2015). Suprathermal particles in XUV-heated and extended exoplanetary upper atmospheres. In H. Lammer & M. Khodachenko (Eds.), *Characterizing stellar and exoplanetary environments*. Astrophysics and space science library (Vol. 411, pp. 105–136). Cham, Switzerland: Springer. https://doi.org/10.1007/978-3-319-09749-7_6
- Simon, C., Witasse, O., Leblanc, F., Gronoff, G., & Bertaux, J.-L. (2009). Dayglow on Mars: Kinetic modeling with SPICAM UV limb data. *Planetary and Space Science*, 57(8–9), 1008–1021. <https://doi.org/10.1016/j.pss.2008.08.012>
- Slanger, T. G., Cravens, T. E., Crovisier, J., Miller, S., & Strobel, D. F. (2008). Photoemission phenomena in the solar system. *Space Science Reviews*, 139(1–4), 267–310. <https://doi.org/10.1007/s11214-008-9387-3>
- Steffl, A. J., Young, L. A., Strobel, D. F., Kammer, J. A., Evans, J. S., Stevens, M. H., et al. (2020). Pluto's ultraviolet spectrum, surface reflectance, and airglow emissions. *The Astronomical Journal*, 159(6), 274. <https://doi.org/10.3847/1538-3881/ab8d1c>
- Stevens, M., Evans, J. S., Schneider, N. M., Stewart, A. I. F., Deighan, J., Jain, S. K., et al. (2015). New observations of molecular nitrogen in the Martian upper atmosphere by IUVS on MAVEN. *Geophysical Research Letters*, 42(21), 9050–9056. <https://doi.org/10.1002/2015GL06531>
- Strickland, D. J., Bishop, J., Evans, J. S., Majeed, T., Shen, P. M., Cox, R. J., et al. (1999). Atmospheric ultraviolet radiance integrated code (AURIC): Theory, software architecture, inputs, and selected results. *Journal of Quantitative Spectroscopy and Radiative Transfer*, 62(6), 689–742. [https://doi.org/10.1016/S0022-4073\(98\)00098-3](https://doi.org/10.1016/S0022-4073(98)00098-3)
- Strickland, D. J., Book, D. L., Coffey, T. P., & Fedder, J. A. (1976). Transport equation techniques for the depositions of auroral electrons. *Journal of Geophysical Research*, 81(16), 2755–2764. <https://doi.org/10.1029/JA081i016p02755>
- Strobl, K. H., & Vidal, C. R. (1987). Radiative lifetimes of selected rovibronic triplet levels of the CO molecule. *The Journal of Chemical Physics*, 86(1), 62–70. <https://doi.org/10.1063/1.452592>
- Szajna, W., Kepa, R., & Zachwieja, M. (2004). Reinvestigation of the $B \ ^2\Sigma^+ \rightarrow X \ ^2\Sigma^+$ system in the CO^+ molecule. *The European Physical Journal D-Atomic, Molecular, Optical and Plasma Physics*, 30(1), 49–55. <https://doi.org/10.1140/epjd/e2004-00060-0>

- Tilford, S. G., & Simmons, J. D. (1972). Atlas of the Observed Absorption Spectrum of Carbon Monoxide Between 1060 and 1900 Å. *Journal of Physical and Chemical Reference Data*, 1(1), 147–188. <https://doi.org/10.1063/1.3253097>
- van Dishoeck, E. F., & Black, J. H. (1986). Comprehensive models of diffuse interstellar clouds: Physical conditions and molecular abundances. *Astrophysical Journal Supplement Series*, 62, 109–145. <https://doi.org/10.1086/191135>
- Veibell, V. (2020). v1.0 Ajello-Lab/analysis: First release of Ajello-Lab data analysis scripts. [Data analysis scripts]. <https://doi.org/10.5281/zenodo.4270483>
- Yonker, J. D., & Bailey, S. M. (2020). N₂(A) in the terrestrial atmosphere. *Journal of Geophysical Research: Space Physics*, 125, e2019JA026508. <https://doi.org/10.1029/2019JA026508>
- Zetner, P. W., Kanik, I., & Trajmar, S. (1998). Electron impact excitation of the a ³Π, a' ³Σ⁺, d ³Δ_g, and A ¹Π states of CO at 10.0, 12.5 and 15.0 eV impact energies. *Journal of Physics B: Atomic, Molecular and Optical Physics*, 31(10), 2395–2413. <https://doi.org/10.1088/0953-4075/31/10/025>
- Zobel, J., Mayer, U., Jung, K., & Ehrhardt, H. (1996). Absolute differential cross sections for electron-impact excitation of CO near threshold: I. The valence states of CO. *Journal of Physics B: Atomic, Molecular and Optical Physics*, 29(4), 813–838. <https://doi.org/10.1088/0953-4075/29/4/021>